KEK-CP-11 KEK Preprint 93-180 LAPP-TH-436/93 LPTHE-ORSAY 93/47 December 1993

Jets in photon-photon collisions: from TRISTAN to $\mathrm{J/N\text{-}LC}$

P. Aurenche, J.-Ph. Guillet
Laboratoire de Physique Théorique ENSLAPP * — Groupe d'Annecy
LAPP, IN2P3-CNRS, B.P. 110, F-74941 Annecy-le-Vieux Cedex, France

M. Fontannaz

Laboratoire de Physique Théorique et Hautes Energies † Université de Paris XI, bâtiment 211, F-91405 Orsay Cedex, France

> Y. Shimizu, J. Fujimoto Physics Department, KEK Tsukuba, Ibaraki 305, Japan

K. Kato

Physics Department, Kogakuin University Shinjuku, Tokyo 160, Japan

Abstract

^{*}URA 14-36 du CNRS, associée à l'Ecole Normale Supérieure de Lyon, et au Laboratoire d'Annecy-le-Vieux de Physique des Particules.

[†]URA 63 du CNRS, associée à l'Université de Paris XI.

We study jet production in photon-photon reactions at the next-to-leading logarithm accuracy. Special emphasis is placed on the discussion of the theoretical uncertainties and on the role of the hadronic component of the photon structure function. We also discuss subtleties in the quasi-real photon spectrum when the photon is involved in a large transverse momentum reaction. The phenomenology at TRISTAN energies is discussed and predictions are made for LEP and a 1 TeV e^+ e^- collider.

1 Introduction

Very recently, several experimental collaborations have published results concerning large transverse momenta phenomena in $\gamma - \gamma$ collisions where the incoming photons are real or quasi-real. In particular, the AMY [1] and TOPAZ [2] collaborations have measured the high transverse momentum jet rates at $\sqrt{s_{e^+e^-}} = 58~GeV$. At a lower energy ($\sqrt{s_{e^+e^-}} = 29~GeV$) a related observable, namely the large p_T particle spectrum, has been measured at the MARK II [3] detector. Theoretical work on this subject started long ago [4],[5]. Here for the first time, we discuss the QCD predictions, at the next-to-leading logarithm accuracy, of the production of jets in $\gamma - \gamma$ collisions. This study seems appropriate at this time since the above data are rather precise and, furthermore, data at higher energies are coming from LEP [6]. It is well known that the rate of $\gamma - \gamma$ events increases with energy in contrast to the rate of e^+ e^- annihilation into a virtual photon in the s-channel and therefore $\gamma - \gamma$ large p_T phenomena will provide an increasingly important background in the search of new phenomena at very high energies.

A priori, hard physics in $\gamma - \gamma$ collisions should be very simple since the photon couples directly to the partons involved in the hard momentum transfer process: it is indeed so in the kinematical region where the transverse momentum is not too small compared to the initial energy. However, in the intermediate p_T region the anomalous photon component [7, 8] introduces a new contribution where the photon couples through its perturbative quark and gluon contents. The problem is further complicated by the non-perturbative hadronic component of the photon which is often described in the vector meson dominance model (VDM). The (perturbative) anomalous and the (non-perturbative) hadronic components can be dealt with by introducing the scale dependent photon structure function very much in the same way one introduces a hadron structure function, with the difference that the former is predicted by QCD at very large scales. Consequently $\gamma - \gamma$ physics becomes more complicated than hadron-hadron collision physics since the photon interacts either point-like or via its structure function.

In the following we treat all these processes at the next-to-leading logarithmic accuracy i.e. we include higher order corrections both in the structure function and the hard subprocesses in a consistent way. In the literature, the interaction of the photon through its partonic constituents is often referred to as the "resolved" photon interaction [5]: if this terminology may be appropri-

ate at the leading-logarithmic level its becomes inadequate at the next level of accuracy since the non-leading part of the "resolved" photon contributes to the higher order corrections of the direct photon process.

Information about the photon structure function is obtained from different experiments: the quark distribution is rather well constrained from deep-inelastic scattering of a real photon which is, on the other hand, not very sensitive to the gluon distribution in the photon. Preliminary results at HERA [9, 10] have however shown that it is possible to constrain the gluon distribution at rather small values of the x variable. The same can be said of $\gamma - \gamma$ experiments at TRISTAN and LEP although in a somewhat higher x range because the p_T / \sqrt{s} values probed are larger than at HERA. Thus, by collecting experimental information from all these types of reactions a good determination of the photon structure function should be possible. In particular, the non-perturbative gluon content should soon become under control.

In the next section we set up the formalism and define the differential jet cross section at the next-to-leading logarithmic level. We then make a detailed study of the theoretical ambiguities (choice of renormalization and factorization scales) covering TRISTAN energies to $\sqrt{s_{e^+e^-}} = 1~TeV$. Before making a comparison to the recent TOPAZ results we consider several problems related to the approximations involved in the parametrization of the quasi-real photon flux. In particular, we discuss the accuracy of the Weizsäcker-Williams [11] approximation to describe large p_T phenomena under specific experimental tagging conditions. An effective spectrum is introduced which is smaller than the usual one. Then we argue that the virtuality of the photons in the anti-tag conditions used by TOPAZ are such that form-factor effects have to be taken into account and this further reduce the $\gamma - \gamma$ collision rate. Finally typical predictions for LEP and a 1 TeV collider are given.

2 The formalism

Following the previous discussion, one can naturally separate the single inclusive jet cross section at large p_T according to the type of interaction of the incoming photons in the hard sub-process. If both photons couple directly

to the quarks involved in the hard scattering one defines the "direct" cross section (fig. 1)

$$\frac{d\sigma^D}{d\vec{p}_T d\eta}(R) = \frac{d\sigma^{\gamma\gamma \to jet}}{d\vec{p}_T d\eta} + \frac{\alpha_s(\mu)}{2\pi} K^D(R; M). \tag{1}$$

If one photon only interacts via the quark or the gluon component in its structure function we define (fig. 2)

$$\frac{d\sigma^{SF}}{d\vec{p}_{T}d\eta}(R) = \sum_{i=q,g} \int dx_{1} F_{i/\gamma}(x_{1}, M)$$

$$\frac{\alpha_{s}(\mu)}{2\pi} \left(\frac{d\sigma^{i\gamma \to jet}}{d\vec{p}_{T}d\eta} + \frac{\alpha_{s}(\mu)}{2\pi} K_{i\gamma}^{SF}(R; M, \mu) \right)$$

$$+ \sum_{j=q,g} \int dx_{2} F_{j/\gamma}(x_{2}, M)$$

$$\frac{\alpha_{s}(\mu)}{2\pi} \left(\frac{d\sigma^{\gamma j \to jet}}{d\vec{p}_{T}d\eta} + \frac{\alpha_{s}(\mu)}{2\pi} K_{\gamma j}^{SF}(R; M, \mu) \right) \qquad (2)$$

Finally, if both photons interact via their structure functions we have (fig. 3)

$$\frac{d\sigma^{DF}}{d\vec{p}_T d\eta}(R) = \sum_{i,j=q,g} \int dx_1 dx_2 F_{i/\gamma}(x_1, M) F_{j/\gamma}(x_2, M)
\left(\frac{\alpha_s(\mu)}{2\pi}\right)^2 \left(\frac{d\sigma^{ij\to jet}}{d\vec{p}_T d\eta} + \frac{\alpha_s(\mu)}{2\pi} K_{ij}^{DF}(R; M, \mu)\right) (3)$$

In writing the above equations we have not specified all the arguments of the various functions but we have kept only those which are relevant for our discussion. The variable R is the usual parameter defining the size of the detected jet with transverse momentum \vec{p}_T , pseudo-rapidity η and azimuthal angle ϕ . When a jet is composed of two partons its coordinates are defined as [12], [2].

$$p_{T} = |\vec{p}_{T_{1}}| + |\vec{p}_{T_{2}}|$$

$$\eta = \frac{1}{p_{T}}(p_{T_{1}}\eta_{1} + p_{T_{2}}\eta_{2})$$

$$\phi = \frac{1}{p_{T}}(p_{T_{1}}\phi_{1} + p_{T_{2}}\phi_{2})$$
(4)

and the condition for the partons to belong to the jet is

$$\sqrt{|\eta_i - \eta|^2 + |\phi_i - \phi|^2} < R. \tag{5}$$

By convention, we have explicitly written the strong interaction coupling out of the partonic cross sections of type $d\sigma^{ij\to jet}/d\vec{p}_T d\eta$ and denoted μ the renormalization scale. The photon structure function $F_{i/\gamma}(x,M)$ is the probability density to find a parton of type i carrying a fraction x of the incoming photon when probed at the factorization scale M. Combinations of structure functions satisfy evolution equations beyond the leading order. If one defines, as usual, singlet and non singlet quark distributions via:

$$\Sigma^{\gamma} = \sum_{f=1}^{N_f} F_{f/\gamma}^+$$

$$F_{f/\gamma}^+ = F_{f/\gamma} + F_{\bar{f}/\gamma}$$

$$F_{f/\gamma}^{NS} = F_{f/\gamma}^+ - \frac{1}{N_f} \Sigma^{\gamma}.$$
(6)

with N_f the number of flavors, the evolution equations can be written

$$\frac{d\Sigma^{\gamma}}{d \ln M^{2}} = k_{q} + P_{qq} \otimes \Sigma^{\gamma} + P_{qg} \otimes F_{g/\gamma},$$

$$\frac{dF_{g/\gamma}}{d \ln M^{2}} = k_{g} + P_{gq} \otimes \Sigma^{\gamma} + P_{gg} \otimes F_{g/\gamma},$$

$$\frac{dF_{f/\gamma}^{NS}}{d \ln M^{2}} = \frac{1}{N_{f}} \left(\frac{e_{f}^{2}}{\langle e^{2} \rangle} - 1\right) k_{q} + P_{NS} \otimes F_{f/\gamma}^{NS}.$$
(7)

The convolution symbol is defined by

$$P \otimes \Sigma^{\gamma} = \int_{x}^{1} dz \ P\left(\frac{x}{z}\right) \ \Sigma^{\gamma}(z) \tag{8}$$

and the average charge squared is

$$\langle e^2 \rangle = \frac{1}{N_f} \sum_{f=1}^{N_f} e_f^2.$$
 (9)

We come back to the discussion of these equations shortly. In eqs. (1)-(3) the functions K^D , K^{SF} and K^{DF} are the higher order corrections to the various

cross sections. These functions depend on the kinematical variables (not shown) as well as the renormalization and factorization scales as indicated. The term K^{DF} is the same as the higher correction term in the production of a large p_T jet in hadron-hadron collisions: it has already been calculated [13]. As for K^{SF} and K^D they are obtained using the same technics as those necessary to obtain K^{DF} starting from the appropriate matrix elements which can be found in [14]. For a precise discussion on the factorized form of eqs. (1)-(3) see [15]. It should be noted that eq. (1) is of order $\alpha_s(\mu)$ while eq. (3) is of order $\alpha_s^3(\mu)$. However, since the structure functions $F_{i/\gamma}(M)$ are known to be of order $\alpha_s^{-1}(M)$ all the equations are in fact calculated consistently up to order α_s when both M and μ large.

As we are now going to discuss, a compensation in the unphysical factorization mass M dependence occurs between the different equations so that each individual equation is not a physical quantity but only the sum of all three equations is the physical observable. In other words, one should not try to associate, for example, eq. (2) to the one-resolved photon cross section since the M scale ambiguity in this quantity occurs at the order at which the calculation is made.

In eqs. (7), the functions P_{ij} , P_{NS} and k_i admit a perturbative expansion of the form

$$P_{ij} = \frac{\alpha_s(M)}{2\pi} \left(P_{ij}^{(0)} + \frac{\alpha_s(M)}{2\pi} P_{ij}^{(1)} \right),$$

$$k_i = \frac{\alpha}{2\pi} \left(k_j^{(0)} + \frac{\alpha_s(M)}{2\pi} k_j^{(1)} \right)$$
(10)

The lowest order terms are the usual Altarelli-Parisi splitting function (with $P_{qq}^{(0)} = P_{NS}^{(0)}$) appearing in the evolution equation of the hadronic structure function. The inhomogeneous coefficient $k_i^{(0)}$ are easily calculated and originate from the splitting of the photon into a collinear quark-antiquark pair at the 0^{th} order in QCD (the so-called box approximation). It is found

$$k_g^{(0)}(x) = 0$$

$$k_q^{(0)}(x) = 2N_c N_f < e^2 > \left(x^2 + (1-x)^2\right)$$

$$= 2N_f P_{q\gamma}^{(0)}(x)$$

$$= 2N_f P_{\bar{q}\gamma}^{(0)}(x)$$
(11)

The corresponding higher order terms can be found in ref. [16] with corrections first discussed in ref. [17]. To illustrate the scale compensation mechanism it is enough to use eqs. (7) to leading order. The discussion is further simplified if we consider only one type of quark so that, for our purposes, the evolution equations reduce to (where we have used for notational convenience $P_{q\gamma}^{(0)} = k_q^{(0)}$)

$$\frac{dF_{i/\gamma}}{d\ln M^2} = \frac{\alpha}{2\pi} P_{i\gamma}^{(0)}(x) + \frac{\alpha_s(M)}{2\pi} P_{ij}^{(0)} \otimes F_{j/\gamma}$$
 (12)

where the label i refers to a quark, an anti-quark or a gluon. The higher order calculation yields the following factorization and renormalization mass scale dependence for the correction terms:

$$\begin{split} K^D &= \frac{\alpha}{2\pi} P_{q\gamma}^{(0)} \otimes \left[\frac{d\sigma^{q\gamma \to jet}}{d\vec{p}_T d\eta} + \frac{d\sigma^{\gamma q \to jet}}{d\vec{p}_T d\eta} \right] \ln \frac{p_T^2}{M^2} + \kappa^D \\ K_{i\gamma}^{SF} &= \left[\frac{\alpha}{2\pi} P_{j\gamma}^{(0)} \otimes \frac{d\sigma^{ij \to jet}}{d\vec{p}_T d\eta} + P_{ij}^{(0)} \otimes \frac{d\sigma^{j\gamma \to jet}}{d\vec{p}_T d\eta} \right] \ln \frac{p_T^2}{M^2} + b \frac{d\sigma^{i\gamma \to jet}}{d\vec{p}_T d\eta} \ln \frac{\mu^2}{p_T^2} + \kappa_{i\gamma}^{SF} \\ K_{ij}^{DF} &= \left[P_{ik}^{(0)} \otimes \frac{d\sigma^{kj \to jet}}{d\vec{p}_T d\eta} + P_{jl}^{(0)} \otimes \frac{d\sigma^{il \to jet}}{d\vec{p}_T d\eta} \right] \ln \frac{p_T^2}{M^2} + 2b \frac{d\sigma^{ij \to jet}}{d\vec{p}_T d\eta} \ln \frac{\mu^2}{p_T^2} + \kappa_{ij}^{D} 13) \end{split}$$

where the numerical coefficient b controls the evolution of the strong coupling at the leading order $(2\pi d\alpha_s(\mu)/d\ln(\mu^2)) = b\alpha_s^2(\mu)$. A change in the factorization scale M of the structure function $F_{i/\gamma}$ induces, according to eq. (12), an inhomogeneous variation controlled by $P_{i\gamma}^{(0)}$ and an homogeneous one proportional to $\alpha_s P_{ij}^{(0)}$. The induced variation on $d\sigma^{SF}/d\vec{p}_T d\eta$ is then compensated, on the one hand, by the term in K^D proportional to $\ln(p_T^2/M^2)$ as far as the inhomogeneous piece is concerned and, on the other hand, by the terms in K^{SF} containing $P_{ij}^{(0)}$ as far as the homogeneous variation is concerned. The remaining terms in K^{SF} linear in $\ln(p_T^2/M^2)$ serve to balance the inhomogeneous variation of $d\sigma^{DF}/d\vec{p}_T d\eta$ whereas the homogeneous variation is compensated by the M dependent terms of K^{DF} . This can be checked explicitly by using eq. (12) to study the variation of eqs. (1)-(3) under a change of M, keeping the renormalization scale μ fixed. As a consequence it is obvious that the sum of the D, SF and DF processes have a physical meaning at the next-to-leading logarithm level since, for this combination, the factorization scale ambiguity is removed at the order at which the calculation is performed.

The effect of a variation of the scale μ is more traditional since the compensation mechanism takes place between the lower order and the higher order terms of the SF and DF cross sections individually exactly as it is the case for purely hadronic reactions. There is no compensation in $d\sigma^D/d\vec{p}_T d\eta$ but the ambiguity appears at the next-to-next-to leading logarithm level.

We finally need to specify the functions $F_{i/\gamma}$, i.e. the parton distributions in the photon which appear in eqs. (2)-(3). These functions are discussed in great details in [15] and we will not dwell on this point here. We just recall that we use the \overline{MS} convention for the structure functions as well as the higher order terms. Furthermore, these functions which are solutions of eqs. (7) are the linear combinations of a (perturbative) anomalous term which is chosen to vanish below the scale $Q_0^2 = .5 \text{ GeV}^2$ and (non-perturbative) hadronic term, related via the usual VDM assumptions to the vector meson structure functions (identified in a first approximation with the pion structure functions). These distributions are in good agreement with the data on F_2^{γ} from PLUTO [18], AMY [19], JADE [20].

We illustrate the above discussion by plotting, for a few relevant examples (see figs. 4 and 5), the variation of the theoretical cross section under independent changes of the scales M and μ . The figures are obtained using the standard photon structure functions [15] and after folding the $\gamma - \gamma$ cross section with the appropriate Weizsäcker-Williams spectrum to reconstruct the observable $e^+e^- \rightarrow jet$ as is explained in detail in the next section. We show the result for TOPAZ, $\sqrt{s_{e^+e^-}} = 58 \; GeV$ and $p_T = 5.24 \; GeV/c$, as well as for $\sqrt{s_{e^+e^-}}=1~TeV$ and $p_T=50~GeV/c$. The general features are the following: as expected the leading logarithm predictions are monotonously increasing when M increases and μ decreases whereas the next-to-leading logarithm predictions have, in general, a maximum in μ at a fixed factorization scale. Unfortunately, there is no optimum in the variable M for a fixed renormalization scale except at unrealistically low μ . This is due to the extremely rapid variation of the DF term, eq. (3), which is only partially compensated by the variation of the SF term in the opposite direction. As a result there does not exist a region of stability (saddle point or absolute maximum or minimum) of the cross section under changes of scale as is often found in other perturbatively calculated QCD processes. We nevertheless observe that the next-to-leading logarithm cross section is considerably flatter than the leading logarithm one for $\mu > 1$ GeV in the case of TOPAZ and $\mu > 3 \; GeV$ in the case of J/N-LC. We can also observe that keeping the ratio μ/M fixed and changing the common scale both the leading and the next-to-leading cross sections are surprisingly stable: this is due to the compensation of the logarithmic dependence of the anomalous component by the strong interaction coupling. The value of the cross sections however depends on the value of the ratio of the two scales. In the following, we will use the standard choice $\mu=M$, keeping in mind the rather large uncertainty in the theoretical predictions.

3 Phenomenology and comparison with TOPAZ data

The discussion in the previous section concerns jet production in collisions between two real photons. The experimental situation is not so simple since the measurements are done for jet production in e^+e^- via the exchange of two quasi-real photons. We discuss now the method and the approximations involved in going from the theoretical results to the experimental observables. The basic formula relating these two quantities relies on the equivalent photon approximation or the Weizsäcker-Williams approximation [11] which factorizes the flux of quasi-real photons emitted by the electron and the positron from the interaction rate between the two photons assumed to be real

$$\frac{d\sigma^{e^+e^-\to jet}}{d\vec{p}_T d\eta} = \int dz_1 dz_2 F_{\gamma/e}(z_1, E) F_{\gamma/e}(z_2, E) \frac{d\sigma^{\gamma\gamma\to jet}}{d\vec{p}_T d\eta}$$
(14)

where E is the common energy of the electron and the positron. It has been shown that the expression [21]

$$F_{\gamma/e}(z,E) = \frac{\alpha}{\pi z} \left(\left(1 + (1-z)^2 \right) \left(\ln \frac{2(1-z)E}{m_e} - \frac{1}{2} \right) - \frac{z^2}{2} \left(\ln z - 1 \right) - \frac{(2-z)^2}{2} \ln(2-z) \right)$$
(15)

is a good approximation for total as well as differential rates in the case of no-tag experiments. With a slight simplification, the anti-tag condition of TOPAZ [2] excludes events with an electron or a positron with a polar angle larger than 3.2° and the above approximation overestimates the rate of

photons [22]. To illustrate this consider, for example, the reaction $e^+e^- \to e^+e^-\mu^+\mu^-$ to the lowest order in QED. In fig. 6, the differential cross section in p_T of a muon is evaluated with the exact matrix element and compared with the estimate based on eqs. (14) and (15): the latter prediction exceeds the former one by approximately 10% for $p_T = 2~GeV/c$ and by as much as 100% at the largest p_T values. Under the experimental conditions of TOPAZ a much better approximation is based on the following form

$$F_{\gamma/e}(z,E) = \frac{\alpha}{2\pi z} \left(1 + (1-z)^2 \right) \int_{Q_{min}^2}^{Q_{max}^2} \frac{dQ^2}{Q^2}$$
 (16)

appropriate for small angle scattering and which explicitly exhibits the dependence on the photon propagator. The boundary conditions Q_{min}^2 and Q_{max}^2 on the photon virtuality depend on the experimental triggering conditions. For an anti-tag condition defined by an angle θ_{max} one has $Q_{min}^2 = m_e^2 z^2/(1-z)$ and $Q_{max}^2 = E^2 \theta_{max}^2 (1-z)$ so that the appropriate Weizsäcker-Williams spectrum becomes

$$F_{\gamma/e}(z, E) = \frac{\alpha}{\pi z} \left(1 + (1 - z)^2 \right) \ln \frac{(1 - z)E\theta_{max}}{z \ m_e}$$
 (17)

In that case, the approximation overestimates the true result by about roughly 8% independently of p_T up to 8.5 GeV/c. We shall therefore base our predictions on eq. (17) taking into account this small correction factor. Strictly speaking, this procedure is accurate for the direct production of jets eq. (1) which are produced via the same diagrams as the muons in the above example. Because of the delicate compensation mechanism between eqs. (1)-(3) discussed in the previous section, we have to use the same Weizsäcker-Williams spectrum for all three types of reactions, at least for those parts depending on the anomalous structure functions. This turns out to be justified as can be seen from the following arguments based on a leading logarithmic analysis. The new feature in the SF and DF components compared to the direct process is the logarithmic dependence of the anomalous photon structure function. The usual behavior in $\ln(M^2/Q_0^2)$ is correct when the photon virtuality Q^2 is small, say $Q^2 < Q_0^2$, (where we recall that Q_0 is the scale below which the perturbative component vanishes). When the virtuality of the photon exceeds this bound it is Q^2 which acts as the cut-off and the photon structure function behaves then as $\ln(M^2/Q^2)$ [23]. Introducing this

factor in eq. (16) and using the anti-tag condition we find for the effective photon spectrum

$$F_{\gamma/e}(z,E) = \frac{\alpha}{2\pi z} \left(1 + (1-z)^2 \right) \left(\ln \frac{M^2}{Q_0^2} \ln \frac{Q_{max}^2}{Q_{min}^2} - \frac{1}{2} \ln^2 \frac{Q_{max}^2}{Q_0^2} \right)$$
(18)

The first term is the appropriate spectrum for a real photon interacting through its anomalous component while the second term is the correction factor induced by the virtuality of the exchanged photon. For the experimental conditions of TOPAZ this correction never exceeds 2% and we therefore neglect it altogether.

It remains finally to discuss the effect of the non-perturbative component. According to the VDM hypothesis and using the one-pole approximation the hadronic photon propagator is of the type $m^2/(q^2(q^2-m^2))$ rather than the usual $1/q^2$ form. The parameter m is the mass of a typical vector meson ρ , ω , ϕ and we simply choose $m^2 = .5 \ GeV^2$ in our model. Neglecting a further q^2 dependence of the structure function of the hadronic photon we defined an effective spectrum according to eq. (16)

$$F_{\gamma/e}(z,E) = \frac{\alpha}{2\pi z} \left(1 + (1-z)^2 \right) \int_{Q_{min}^2}^{Q_{max}^2} \frac{dQ^2}{Q^2} \left(\frac{m^2}{Q^2 + m^2} \right)^2$$

$$= \frac{\alpha}{\pi z} \left(1 + (1-z)^2 \right) \left[\ln \frac{(1-z)E\theta_{max}}{z \ m_e} - \frac{1}{2} \left(\ln \left(1 + \frac{(1-z)E^2\theta_{max}^2}{m^2} \right) + \frac{(1-z)E^2\theta_{max}^2}{m^2 + (1-z)E^2\theta_{max}^2} \right) \right]$$

Compared to eq. (17) appropriate for a point-like photon we find for the hadronic photon a suppression factor of the order of 10% - 12% in the kinematic range covered by TOPAZ. It is to be noted that for a no-tag experiment the suppression factor of the VDM component is even bigger since no large $\ln(E/m_e)$ is left in the above formula which reduces at very high energy to

$$F_{\gamma/e}(z,E) = \frac{\alpha}{2\pi z} \left(1 + (1-z)^2 \right) \left[\ln \frac{(1-z)m^2}{z^2 m_e^2} - 1 \right]$$
 (20)

We are now in a position to make a comparison with the data. This is shown in fig. 7. The theoretical predictions are based on different choices for the VDM input: the top curve is obtained when the standard set of structure functions of [15] is used while the bottom curve is the result when one arbitrarily takes the non-perturbative input to be 0 in the standard set. The first remark to be made is the important role played by the nonperturbative component at least at the low p_T end of the spectrum. We have also shown in the figure, as the intermediate curve, the predictions when one arbitrarily divides the normalization of the hadronic term by a factor 2, a solution which is still consistent with the data on F_2^{γ} [15]. Let us note that for $p_T > 4 \ GeV/c$ the data (with statistical and systematic errors added linearly) are in very good agreement with all the theoretical curves while for smaller values the standard set of structure function overestimates the data and the no-VDM set, although compatible, is somewhat on the low side. To further test the sensitivity of the non-perturbative input we have also tried to modify the shape of the quark and the gluon distributions in the VDM component keeping the overall normalization as in the standard set and we have found that the predictions vary very little, at most by a few %: it thus appears that jet data in $\gamma - \gamma$ collisions are not very sensitive to the details of the parton distributions due to the extra convolutions involved in going from $\gamma - \gamma$ data to e^+e^- data. This is illustrated in fig. 8 where we show the effective $xF_{u/e}^+(x)$ quark and $xF_{g/e}(x)$ gluon momentum weighted distributions in the electron as "seen" at TOPAZ. These curves are obtained by taking the convolution of the parton densities in the photon, at a fixed factorization scale, with the Weizsäcker-Williams spectrum appropriate to the experimental triggering conditions. The two sets of curves in each figure correspond to harder and softer parton distributions, than the standard ones, in the hadronic component of the photon. We choose

$$xv(x, 2GeV^2) \simeq (1-x)^{.85}$$

 $xG(x, 2GeV^2) \simeq (1-x)^1$ (21)

for the hard set and

$$xv(x, 2GeV^2) \simeq (1-x)^2$$

$$xG(x, 2GeV^2) \simeq (1-x)^3$$
 (22)

for the soft set. In each case the normalization factors are appropriately chosen to satisfy the known sum rules. We recall that the standard parametriza-

tion, as fitted to the pion induced hard cross sections [24], is

$$xv(x, 2GeV^2) \simeq (1-x)^{.85}$$

 $xG(x, 2GeV^2) \simeq (1-x)^{1.94}$ (23)

We note that the two extreme sets are very similar in the region $x \simeq .2$. Since the effective x probed by TOPAZ is estimated to be $x \simeq .15$ at $p_T = 3~GeV/c$ and $x \simeq .25$ at $p_T = 7~GeV/c$, it is not surprising that the data are rather insensitive to changes in the shape of the hadronic component.

It may be interesting to discuss at this point the role of the next-to-leading logarithm (NTL) corrections. The comparison with the leading logarithm (LL) results is made using the same scale $\mu = M = p_T$ and the standard set of structure functions. Thus we discuss only the size of the correction factors K^D , K^{SF} and K^{DF} of eq. (13). Globally we find that the NTL corrections increase the cross section by 25% at $p_T = 3 \text{ GeV/c}$ and only 3% at $p_T = 7.5 \; GeV/c$. The higher order terms affect the components rather differently since the direct cross section is reduced by 15% throughout the p_T range covered by the data, the SF one is left approximately unchanged (a few % variation) and the DF one increases by 70%. The net result of this pattern of corrections is that the direct cross section is reduced from 35% to 24% of the total jet cross section at $p_T = 3.12 \text{ GeV/c}$ and from 51% to 42% at $p_T = 7.5 \; GeV/c$. Let us note finally the relative importance of the DF term since it accounts for 55% of the total at $p_T = 3.12 \; GeV/c$ and still 31% at $p_T = 7.5 \; GeV/c$ Needless to say that all these figures would be affected had we used a different jet definition.

The discrepancy between theory and experiment at low p_T may, after all, not be too surprising. Because of the smallness of the scales involved the perturbative regime may not have set in. In other words, non-perturbative intrinsic p_T effects, which have been ignored in our calculation, could somewhat affect the theoretical predictions. More probably however, the relevant point is the neglect of the charm quark mass in the hard partonic cross sections as well as in the evolution of the structure functions except for the charm threshold at $M^2 = 2 \text{ GeV}^2$. An estimate of this effect may be attempted by comparing, in the leading logarithmic approximation, the direct cross section using four massless quarks with that assuming three massless flavors and a charm quark of mass $1.5 \text{ GeV}/c^2$. In the latter case, the cross section is reduced by 14% at $p_T = 3 \text{ GeV}/c$, 5% at $p_T = 5 \text{ GeV}/c$ and only

2% at $p_T = 7~GeV/c$. Such factors when applied to our predictions would put the two VDM curves in perfect agreement with the data and disfavor the no-VDM predictions. Of course such corrections factors are only indicative since the physics of jet production is much more complex than the simple direct production specially at small transverse momentum.

In fig. 9 we show the predictions for the jet p_T spectrum at LEP 200 with a no-tag condition and in fig. 10 those at a collider with an energy $\sqrt{s_{e^+e^-}} = 1 \, TeV$. Despite the large scales involved it is interesting to remark that the non-perturbative term still gives a large contribution up to rather high p_T values. This is related to the fact that higher energy experiments tend to probe smaller x values of the photon structure function where the hadronic component is important.

4 Conclusions

Despite the rather large intrinsic scale uncertainties involved in the theoretical predictions for single jet production in $\gamma - \gamma$ collisions, useful phenomenology can be done. Good agreement is obtained with TOPAZ data for $p_T > 4 \ GeV/c$. The rather large error bars (both experimental and theoretical) do not allow, for the moment, to distinguish the predictions based on different sets of structure functions: both the set without a nonperturbative component and the set with the theoretically expected VDM input (standard set) are compatible with the data. For $p_T < 4 \text{ GeV/}c$, the charm mass neglected in the calculation, plays an important role. Correcting semi-quantitatively for this mass effect we find the standard set to be in agreement with the data while the other one gives too small a cross section. Another feature of our work is the importance of higher order corrections to processes where the photon couples through its structure function. This means that at low jet p_T values the direct process is relatively reduced and therefore $\gamma - \gamma$ collisions tend to look like hadron-hadron collisions with some jet activity in the forward and backward direction.

We find it remarkable that QCD is able to correlate in a rather consistent way the measurements on F_2^{γ} to the rate of jet production in $\gamma - \gamma$ collisions. The agreement is even more remarkable if one remembers that the mass scale involved, typically the jet transverse momentum, are rather small. We eagerly wait for more precise data to put the theory to an even more stringent

test.

As seen in our analysis, some complications in the comparison between theory and experiment arose from the virtuality of the photons: theoretical predictions are made for real photons while experiments deal with off-shell photons. This problem can be handled in the framework of the Vector Dominance Model. It would make the comparison between theory and experiment more direct if experimental triggering conditions could be such as to minimize the virtuality of the photons and this wish also applies to measurements of F_2^{γ} as well as of jet production in $\gamma - \gamma$ collisions.

Acknowledgements

We thank H. Hayashii for many informative and helpful discussions as well as N. Nakazawa for early collaboration on this work. We are indebted to CNRS-IN2P3(France) and Monbusho(Japan) for financial support to our collaboration.

References

- [1] AMY collaboration: R. Tanaka et al., Phys. Lett. **B277** (1992) 215.
- [2] TOPAZ collaboration: H. Hayashii et al., Phys. Lett. **B314** (1993) 149.
- [3] MARK II collaboration: D. Cords et al., Phys. Lett. **B302** (1993) 341.
- [4] S.J. Brodsky, T. DeGrand, J. Gunion and J. Weis, Phys. Rev. 19 (1979) 1418;
 - K. Kajantie and R. Raitio, Nucl. Phys. **B159** (1979) 528;
 - S.P. Li and H.C. Liu, Phys. Lett. **143B** (1984) 489;
 - A.V. Efremov, S.V. Ivanov and G.P. Korchemskii, Sov. Jour. Nuc. Phys. **39** (1984) 987;
 - F.A. Berends, Z. Kunszt and R. Gastmans, Nucl. Phys. **B182** (1984) 987.
 - P. Aurenche, R. Baier, A. Douiri, M. Fontannaz and D. Schiff, Z. Phys. C29 (1985) 423.
- [5] M. Drees and R.M. Godbole, Nucl. Phys. B339 (1990) 355;
 M. Drees, preprint DESY 92-065, May 1992, Proceedings of the IXth International Workshop on Photon-Photon collisions, La Jolla, CA, USA.
- [6] ALEPH collaboration: D. Buskulic et al., CERN-PPE-93-94, June 1993.
- [7] E. Witten, Nucl. Phys. **B120** (1977) 189.
- [8] W.A. Bardeen and A.J. Buras, Phys. Rev. **D20** (1979) 166; Phys. Rev. **D21** (1980) 2041 E.
- [9] H1 collaboration: T. Ahmed et al., Phys. Lett. **B297** (1992) 205, T. Abt et al., Phys. Lett. (B314) (1993) 436.
- [10] ZEUS collaboration: M. Derrick et al., Phys. Lett. **B297** (1992) 404.
- [11] C.F. Weizsäcker, Z. Phys. 88 (1934) 612;
 E.J. Williams, Phys. Rev. 45 (1934) 729.
- [12] J.E. Huth et al., FERMILAB-CONF-90-249E, Summer study group on high energy physics, Snowmass, Colorado, USA.

- [13] F. Aversa, P. Chiappetta, M. Greco and J.Ph. Guillet, Nucl. Phys. B327 (1989) 105; Z. Phys. C46 (1990) 401; Phys. Rev. Lett. 65 (1990) 401.
 S.D. Ellis, D. Kunzst and D.E. Soper Phys. Rev. D40 (1989) 2188; Phys. Rev. Lett. 64 (1990) 2121.
- [14] P. Aurenche, R. Baier, A. Douiri, M. Fontannaz and D. Schiff, Nucl. Phys. B286 (1987) 509.
- [15] M. Fontannaz, Orsay preprint LPTHE-93-22, talk given at the 21st International meeting on Fundamental Physics, Miraflores de la Sierra, Spain, May 1993;
 P. Aurenche, M. Fontannaz and J.Ph. Guillet, Orsay preprint LPTHE 93-37, October 1993.
- [16] M.Glück and E. Reya, Phys. Rev. **D28** (1983) 2749;
 M. Glück, E. Reya and A. Vogt, Phys. Rev. **D45** (1992) 3986; Phys. Rev. **D46** (1992) 1973.
- [17] M. Fontannaz and E. Pilon, Phys. Rev. **D45** (1992) 382.
- [18] PLUTO collaboration: Ch. Berger et al., Nucl. Phys. B281 (1987) 363.
- [19] AMY collaboration: T. Sasaki et al., Phys. Lett. **B252** (1990) 491.
- [20] JADE collaboration: W. Bartel et al., Z. Phys. C24 (1984) 23.
- [21] J. Brodsky, T. Kinoshita and H. Terazawa, Phys. Rev. D4 (1971) 1532.
- [22] In fact TOPAZ accepts events at larger polar angles only when the quasi-real photon carries more than 75% of the electron momentum. Such an effect is included in our predictions but it hardly modifies the jet spectrum in the measured transverse momentum range.
- [23] G.A. Schuler, CERN-TH.6427/92, proceedings of the DESY workshop on physics at HERA, Hamburg, Oct. 1991;
 F.M. Borzumati and G.A. Schuler, Z. Phys. C58 (1993) 139.
- [24] P. Aurenche, R. Baier, M. Fontannaz, M.N. Kienzle-Focacci and M. Werlen, Phys. Lett. B233 (1989) 517.

Figure Captions

- Fig. 1 Direct processes in $\gamma \gamma$ collisions.
- Fig. 2 SF type processes in $\gamma \gamma$ collisions.
- Fig. 3 DF type processes in $\gamma \gamma$ collisions.
- Fig. 4 Variation of the cross section $\frac{d\sigma^{e^+e^-\to jet}}{d\vec{p}_T d\eta}$ at $\sqrt{s}_{e^+e^-} = 58~GeV$, $p_T = 5.24~GeV/c$, $\eta = 0$, with the factorization scale M and the renormalization scale μ : a) leading logarithm predictions; b) next-to-leading logarithm predictions. Note that in order to fully display the shape of the surface we rotated the figure by 90^0 compared a).
- Fig. 5 The same as fig. 1 for $\sqrt{s_{e^+e^-}}=1~TeV,~p_T=50~GeV/c.$
- Fig. 6 Study of the equivalent photon approximation. p_T spectrum of the muon in the process $e^+e^- \to e^+e^-\mu^+\mu^-$ at $\sqrt{s_{e^+e^-}} = 58~GeV$. The data points are the result of the exact calculation, the top line is the no-tag prediction using the Weizsäcker-Williams approximation eq. (15) and the bottom line is from eq. (17) with $\theta_{max} = 3.2^{\circ}$.
- Fig. 7 TOPAZ data on inclusive jet production and theoretical predictions for $\int_{.7}^{.7} d\eta \frac{d\sigma^{e^+e^-\to jet}}{dp_T d\eta}$. The small error bars are statistical(a) and the large ones are statistical and systematic errors added linearly(b). The top curve is the theoretical prediction based on the standard photon structure functions, the middle one is based on structure functions with half the VDM input, and the lower one is based on the perturbative component only.
- Fig. 8 Distributions of a) quarks and b) gluons in the electron under TOPAZ triggering conditions. The solid curve corresponds to the hard input and the dashed one to the soft input. The factorization scale is $M^2 = 25 \ GeV^2$.
- Fig. 9 Single jet production, via the two-photon mechanism, at LEP 200 for a no-tag experiment and $\eta = 0$. The top and bottom curves have the same meaning as in fig. 7.
- Fig. 10 Same as in fig. 9 at $\sqrt{s_{e^+e^-}} = 1 \ TeV$.

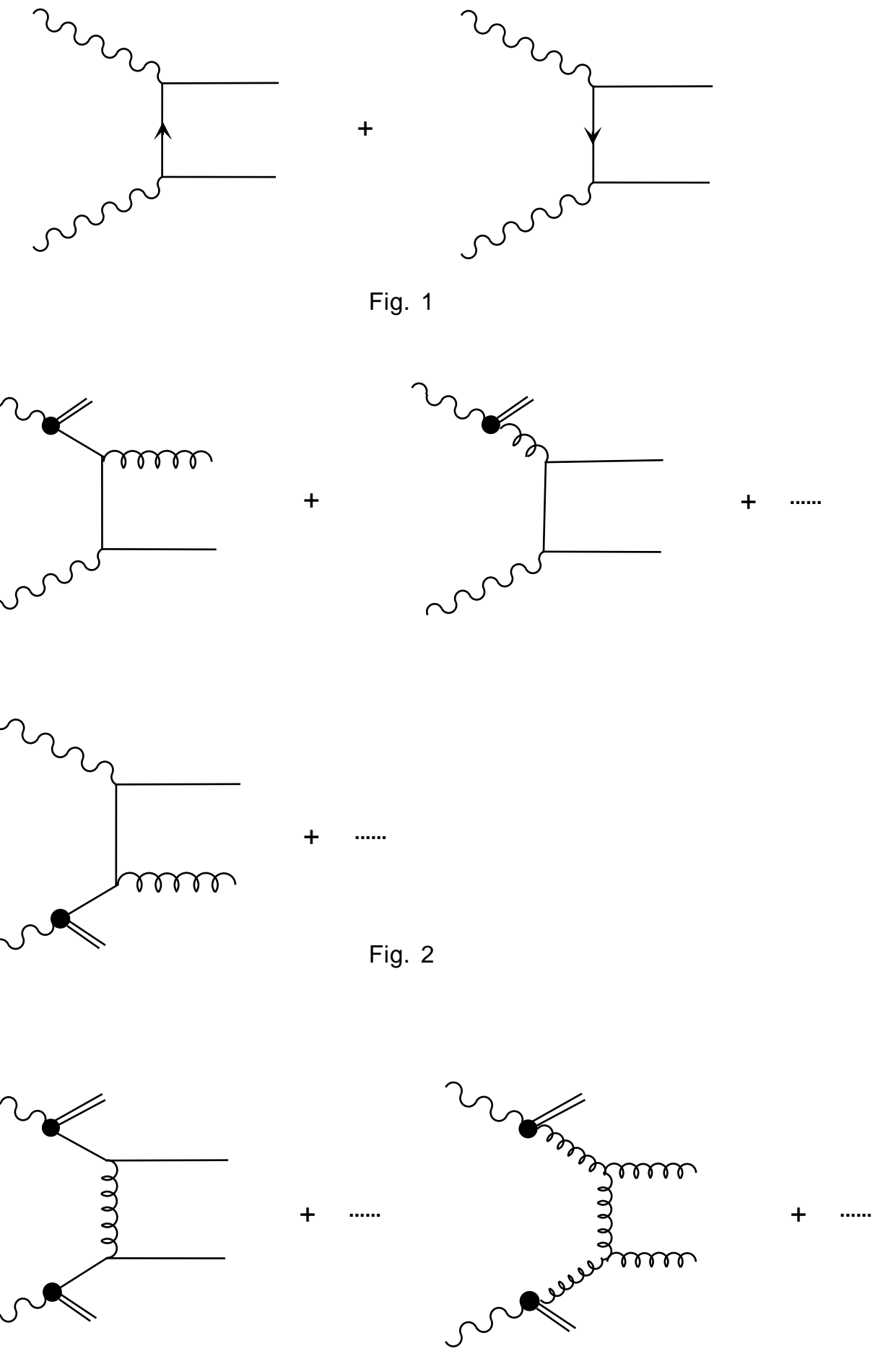


Fig. 3

This figure "fig1-1.png" is available in "png" format from:

This figure "fig2-1.png" is available in "png" format from:

This figure "fig3-1.png" is available in "png" format from:

This figure "fig1-2.png" is available in "png" format from:

This figure "fig2-2.png" is available in "png" format from:

This figure "fig3-2.png" is available in "png" format from:

This figure "fig1-3.png" is available in "png" format from:

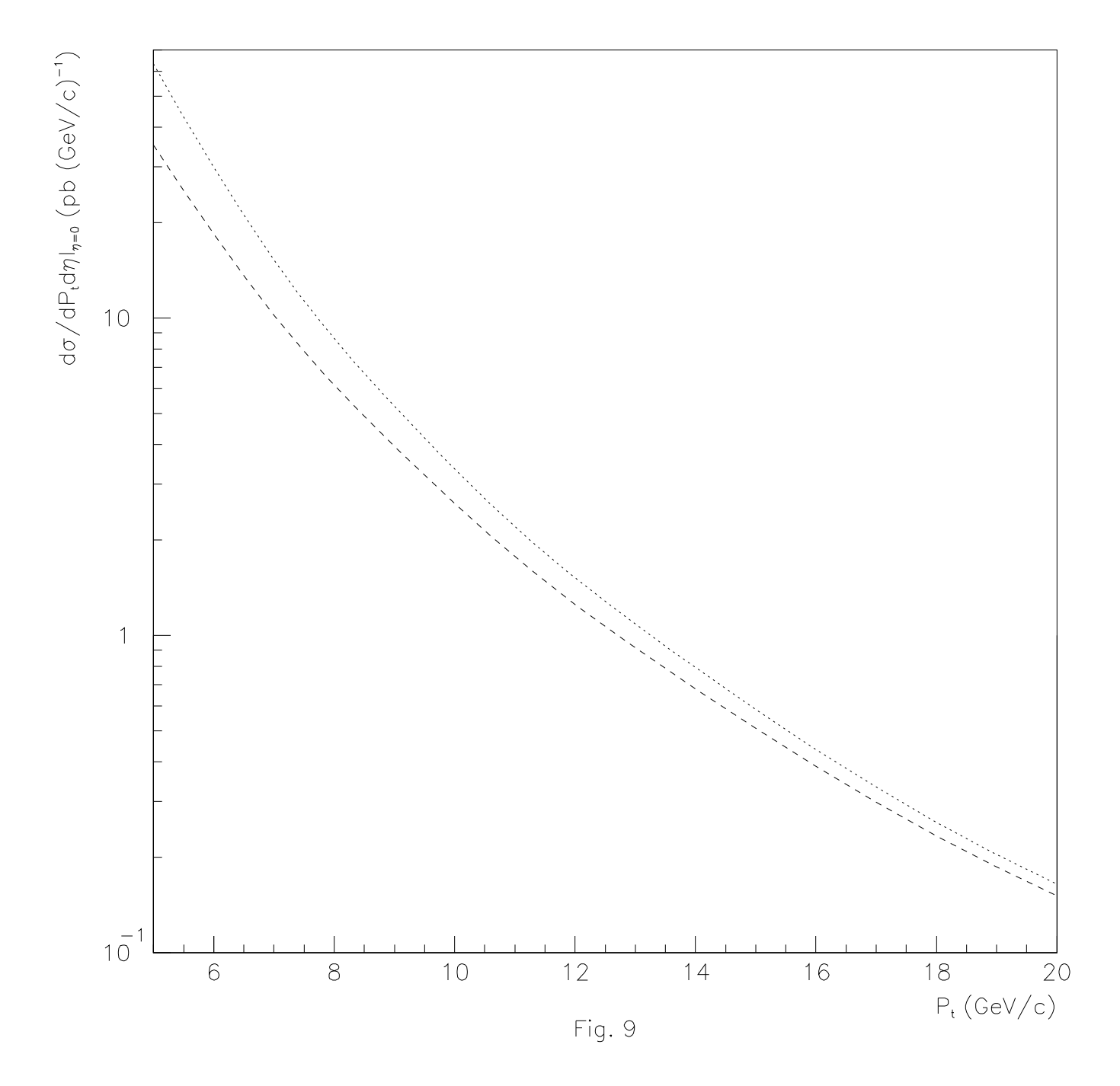
This figure "fig2-3.png" is available in "png" format from:

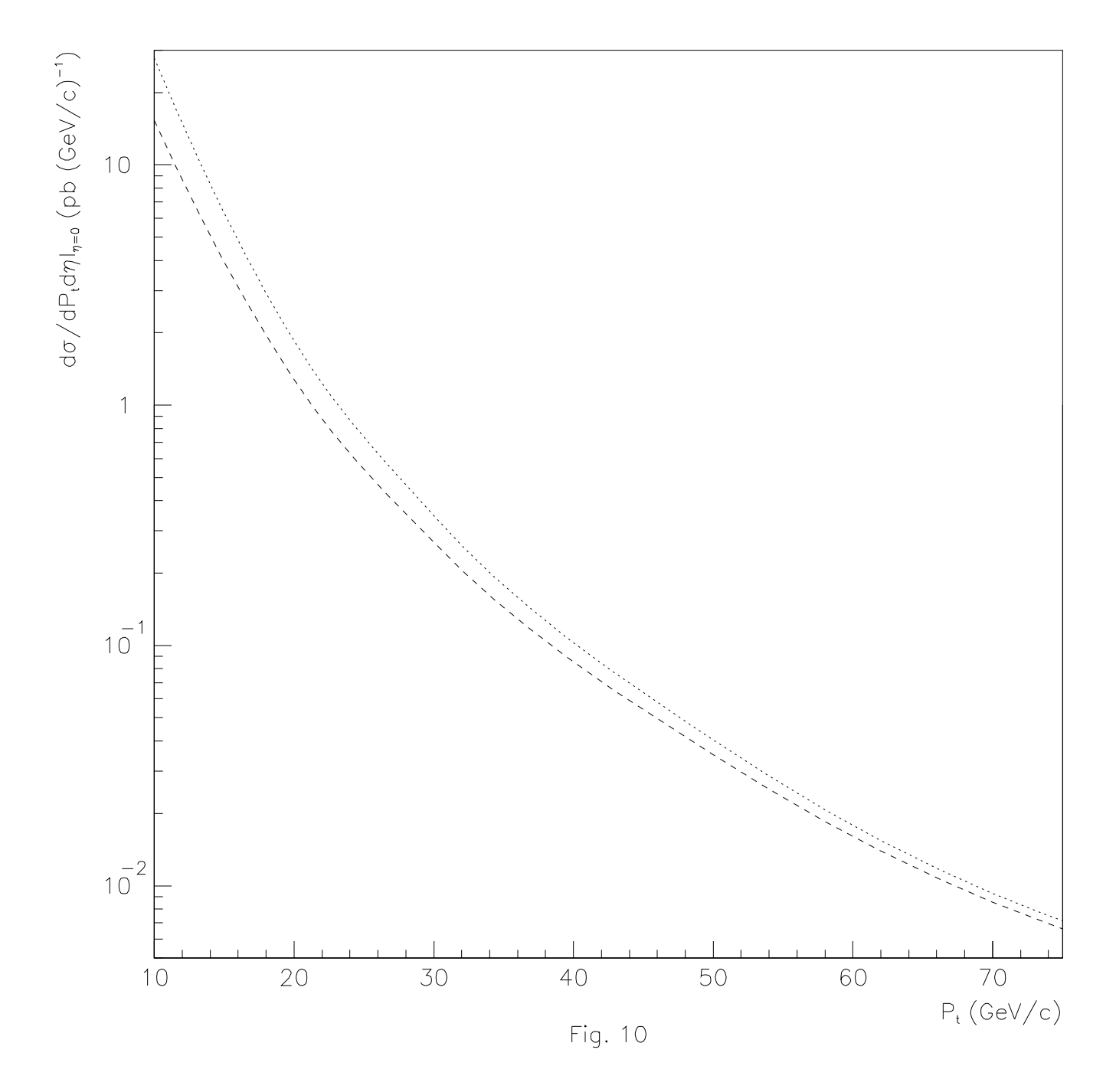
This figure "fig3-3.png" is available in "png" format from:

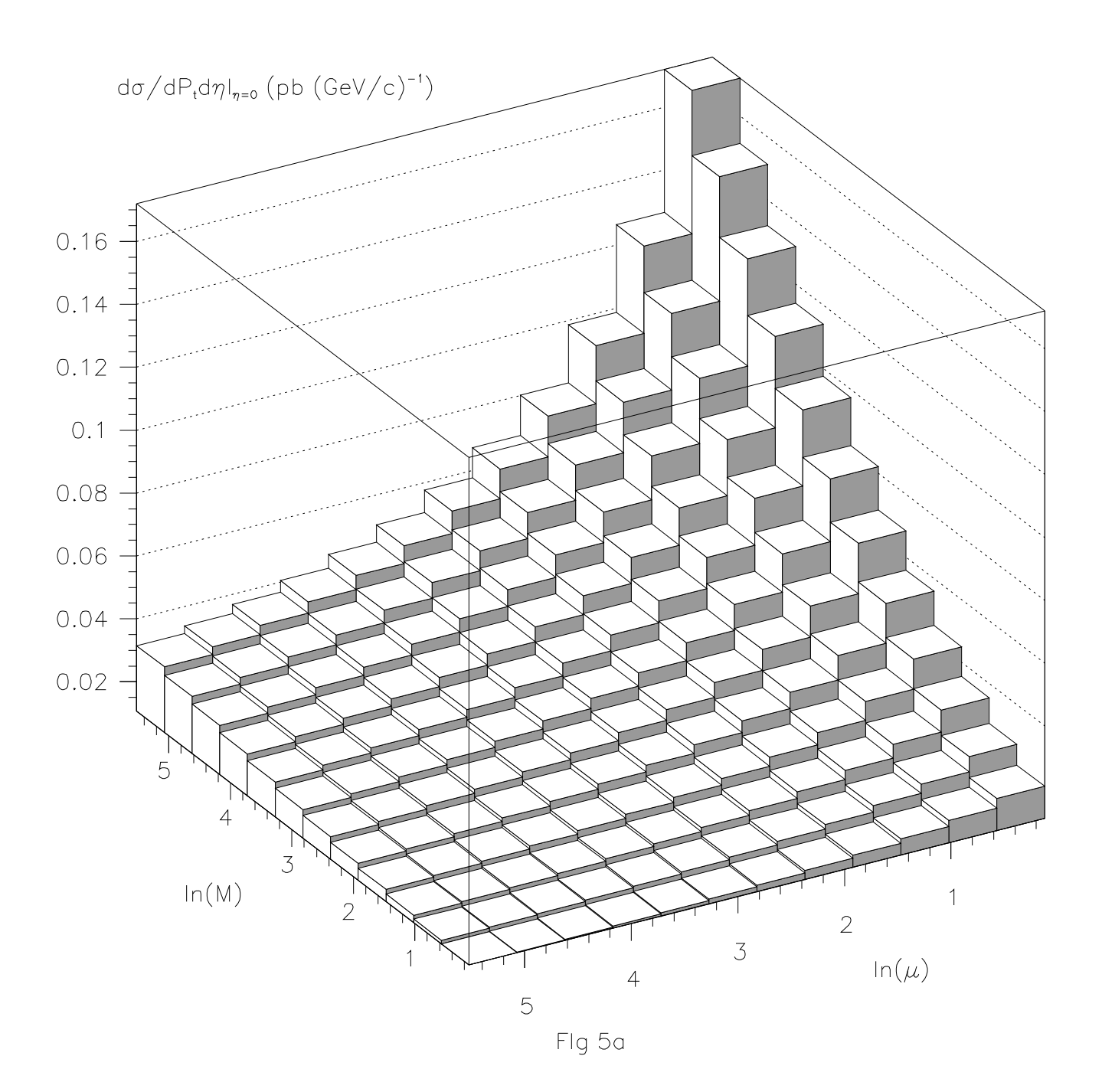
This figure "fig1-4.png" is available in "png" format from:

This figure "fig2-4.png" is available in "png" format from:

This figure "fig3-4.png" is available in "png" format from:







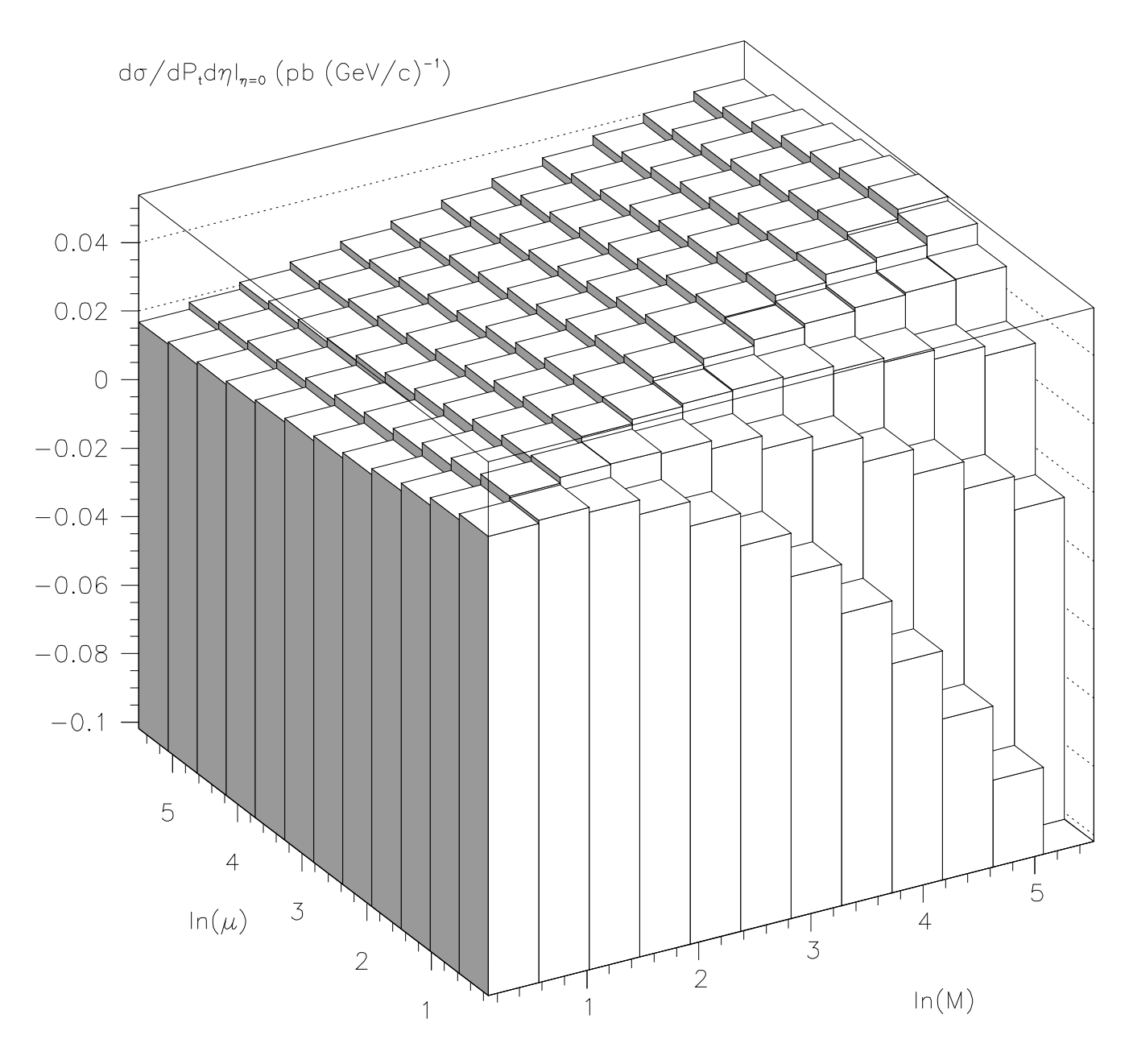


Fig 5b

